Impedance Modelling for High Frequency Unitraveling-Carrier Photodiodes

Marcel Grzeslo and Andreas Stöhr
Zentrum für Halbleitertechnik und Optoelektronik
University of Duisburg Essen
Duisburg, Germany
marcel.grzeslo@uni-due.de

Carlos Biurrun-Quel
Antenna Group. Institute of Smart Cities
Public University of Navarra
Pamplona, Spain
ORCID: 0000-0001-6446-3248

***Abstract*— High-speed photodiodes stand out as potential candidates to enable next-generation communication systems working as mmWave/THz sources due to their intrinsic broadband behaviour. Impedance matching is an essential task in microwave engineering that enables an efficient delivery of the power generated by the source (i.e. photodiode) to the load (i.e. antenna). In this work, we analyse the impedance of a generic uni-travelling carrier photodiode and its dependency with frequency, bias voltage and other operational parameters. In addition, we present some calculations and use cases, highlighting the importance of properly matching this impedance in an actual system.**

Keywords—uni-travelling carrier photodiode, UTC-PD, impedance matching, equivalent circuit

I. INTRODUCTION

The advent of next generation communication systems, with increasing demands in terms of latency and data rates (not only the ones delivered to end-users, but also backhaul links in between the base stations), pushes the efforts to find and develop new systems capable of complying with such stringent demands. The most straightforward way to increase the capacity (C) of a communication channel is to increase the bandwidth available (B), following Shannon-Hartley's Theorem (Eq.1), where S/N is the Signal-to-Noise ratio of the channel.

$$C = B \cdot \log_2(1 + \frac{S}{N}) \tag{1}$$

In order to provide such larger bandwidth, higher frequencies (above 60 GHz and up to 0.3 THz) offering several GHz bandwidths, are requested. Within this context, high-speed photonic detectors, such as photodiodes working as photonic mixers (beating two optical wavelengths to generate the difference-frequency at several tens or hundreds of GHz) arise as highly suitable candidates, offering large bandwidths with reasonable output powers at mmWave/THz frequencies. In particular, Uni-Travelling Carrier Photodiodes (UTC-PD) [1] stand out due to their modified structure, which allows faster responses by avoiding the transportation of holes inside the structure.

Different equivalent circuits have been proposed in the past years for these devices, with some examples found in [2-6]. Whereas they present different degrees of complexity, the common elements in all of them are a series resistor a junction capacitance, which means that a photodiode can be seen as a source with a complex impedance. As a result, maximum transfer of power (MTP) is only achieved when loading the source with the corresponding conjugate impedance. This fact did not received much attention in the literature until recently, with some remarkable works addressing this issue [4-10]. On the other hand, many authors would design and integrate their photodiodes with standard 50 Ω lines or neglect the imaginary part. The effect of not addressing the impedance matching issue can be outlined simply by a rough calculation. Following Eq.2, the magnitude reflection coefficient |Γ| at the interface between the photodiode (with impedance Z_{PD}) and a standard transmission line (with impedance Z_0=50 Ω) can be obtained.

$$|\Gamma| = |\frac{Z_0 - Z_{PD}^*}{Z_0 + Z_{PD}}| \tag{2}$$

Let us assume a sample value of Z_{PD}=20 –j·30 Ω. In this example, (2) leads to a reflection coefficient of 0.557. The power delivered (P_{del}) to the transmission line can be calculated as (3), where P_0 would be the nominal power produced by the PD. As a result, it is observed that about 31 % of the power is being lost due to the impedance mismatch, for this example.

$$P_{del} = P_0 \cdot (1 - |\Gamma|^2) \tag{3}$$

Furthermore, the impedance of the photodiode is not a constant value. It depends not only on the frequency, but also on other parameters such as the bias voltage or the impinging optical power. In this work, we perform a study be means of simulation with the aim to predict these dependencies accurately, in order to avoid losses due to impedance mismatch when integrating UTC-PDs with other components in communication systems.

II. SIMULATION AND RESULTS

A. Device setup and Equivalent circuit

To investigate the effect of optical power on the impedance, simulations of a generic UTC-PD have been carried out using TCAD Atlas. In order to provide realistic charge carrier dynamics, the energy-balance model has been implemented which includes non-local effects resulting into a non-equilibrium or "overshoot" of electrons [12]. The layer structure of the used UTC-PD is presented in table 1 showing all relevant layers together with their doping concentration and thicknesses.

TABLE I. LAYER STRUCTURE OF SIMULATED UTC-PD

Material	Doping concentration	Thickness
p^+-InGaAs	2x10^{19} cm^{-3}	50 nm
p^+-InP	4x10^{18} cm^{-3}	500 nm
p^+-InGaAsP	4x10^{18} cm^{-3}	20 nm
p^+-InGaAs	2 → 0.2x10^{18} cm^{-3}	50 nm
n.i.d.-InGaAs	undoped	60 nm
n. i. d.-InGaAsP	undoped	20 nm
n-InP	1x10^{16} cm^{-3}	150 nm
n^+-InGaAsP	1.5x10^{18} cm^{-3}	350 nm
n^+-InP	1x10^{19} cm^{-3}	1 µm
S.I. InP-substrate	undoped	100 µm

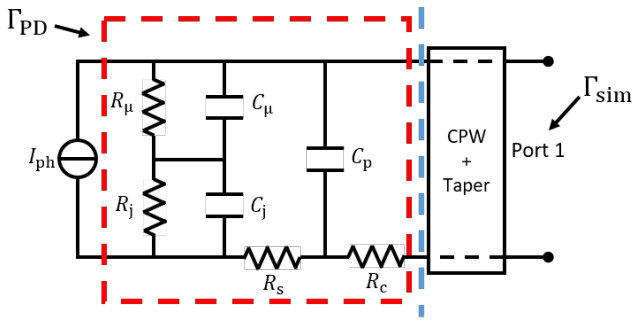

Fig. 1. Equivalent circuit applied for the impedance calculations of the UTC-PD

The UTC-PD has a surface area of 30 µm² and shows a responsivity of 0.63 A/W at a wavelength of 1.55 µm. To further simplify the particular behaviors of the individual layers, a simple equivalent circuit has been used which is oriented to previous works [5]. Here the chemical capacitance C_μ and resistance R_μ refer to the InGaAs-absorber region while the junction capacitance C_j and resistance R_j refer to the collector region where no carrier generation is taking place. Furthermore, the series resistance R_s within the p- and n-regions was estimated to be 6 Ω with an estimated parallel capacitance C_p of 3 fF. The contribution of the contact resistance R_c was negligible in this simulation since they were defined as perfectly ohmic.

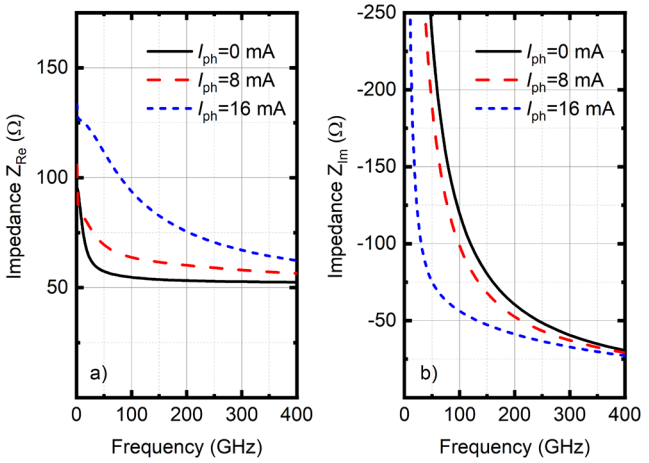

Fig. 2. Real (a) and imaginary (b) part of the impedance extracted from simulated S11-parameters for several photocurrents at a reverse voltage of $U_0 = -1$ V.

The respective real and imaginary part of the impedance has been extracted from simulated S_{11}-parameters as shown in the following equations (4) and (5):

$$Z_R = Z_0 \cdot \frac{1-S_{11,Re}^2-S_{11,Im}^2}{(1-S_{11,Re})^2+S_{11,Im}^2} \quad (4)$$

$$Z_X = Z_0 \cdot \frac{2 \cdot S_{11,Im}}{(1-S_{11,Re})^2+S_{11,Im}^2} \quad (5)$$

Here Z_0 has been set to 50 Ω. After the model has been established, the behavior of the UTC-PD regarding optical power and applied voltage can be investigated. Figure 2 illustrates the altered Impedance for an increasing photocurrent. It reveals an increase in the real part of the impedance while the imaginary part experiences a decrease. The effect is especially dominant for frequencies under 300 GHz and is mainly caused by space-charge screening [5]. Furthermore, this effect can be explained by looking at the carrier accumulation and its influence on the electric field distribution. Figure 3 shows the electron density and electric field profile for several photocurrents at a 1 V reverse bias. Carrier screening usually occurs at the interface between InGaAs and InP layer where the transition of carriers is assisted by thermionic emission accompanied by quantum tunnelling [12]. The accumulation of carriers leads to coulomb screening and results into a reduction of the electric field.

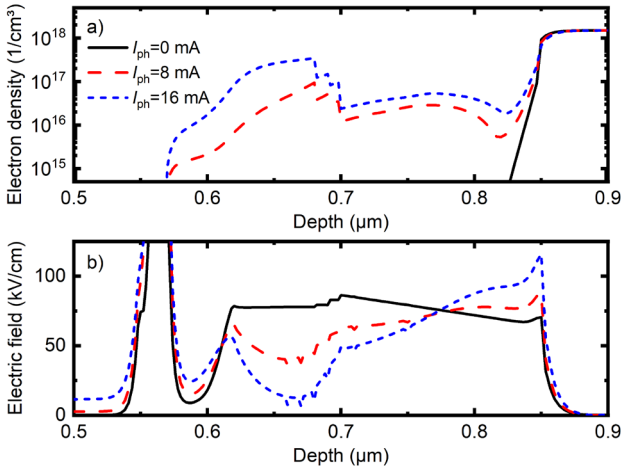

Fig. 3. UTC-PD for a bias voltage of $U_0 = -1$ V showing the electron density in (a) and electric field in (b)

The decrease in electric field occurs majorly within the absorber region, which leads to a nonlinear built up in capacitance. By using the equivalent circuit in Figure 1 the individual components can be extracted by fitting the impedance values shown in Figure 2 using MATLAB.

Modelling the components inside the equivalent circuit of a UTC-PD in dependence of photocurrent and voltage has been already examined in [5]. Figure 4 a) shows one of the fitted values for increasing photocurrent revealing an increase in capacitance C_μ for photocurrent exceeding 5 mA at a reverse bias of -1 V. This seems to correspond to the behaviour mentioned in [5], where capacitances and resistances can be approximated as constant if the photocurrent remains below a certain value before carrier screening takes place. At higher optical powers an increase in capacitance and decrease in resistance occurs. An analytical expression has been derived into equation 6 and 7 showing the behaviour of resistance and capacitance as function of carrier density and voltage [5].

$$C \approx \frac{\varepsilon_0 \varepsilon_r A}{d} + \frac{q_0 d_2 A \cdot \Delta n}{\Delta U} \quad (6)$$

$$R \approx \frac{d_1}{q_0 \mu_n A n_0} + \frac{d_2}{q_0 \mu_n A \cdot (n_0+n)} \quad (7)$$

The respective equations consist of a term which is constant and a term which is indirectly dependent from the photocurrent. With regard to the capacitance the current evokes a variation in carrier density Δn and voltage ΔU within the depletion region. Both lead to a non-linear increase of C_μ which is visible in Figure 4 a). Higher reverse voltages reduce the effect of carrier screening resulting in a much

flatter curve progression. In comparison, the resistance R_μ in Figure 4 b) is dependent on the variation of carrier density only while decreasing after the carrier screening effect becomes dominant. The trends in both graphs are in agreement with equation 6 and 7 offering the possibility of analytically estimating the change in impedance as a function of photocurrent. However, the fitting results of junction capacitance C_j and resistance R_j showed no clear trend which might be caused by a different redistribution of electric field within the collector region as visible in Figure 3 b). Further improvement in fitting the equivalent circuit is necessary for a more reliable model.

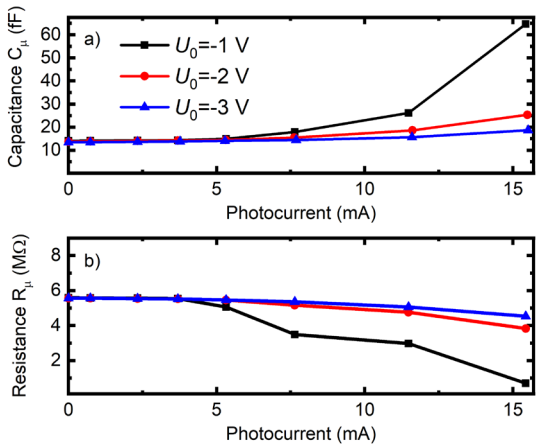

Fig. 4. Fitted values for the Capacitance C_μ (a) and Resistance R_μ (b) for increasing photocurrent and several bias voltages.

Following chapter highlights the benefit of estimating the change in impedance by presenting the transmission losses in case of an occurring impedance mismatching.

B. Calculated losses due to impedance mismatching

The importance of matching the impedance of the photodiode with the antenna was already highlighted by the authors in [4]. However, it is observed that little attention has been paid to this same issue when designing transitions to rectangular waveguides, which is another traditional way of integrating photodiodes in communication systems. One example can be found in [13], where a transition from coplanar waveguide (GCPW) to rectangular waveguide (WR) based on a double-slot structure on the bottom ground is presented. Here, the authors present a scalable solution from 50 GHz to 1.1 THz for a 50 Ω GCPW, although the aim is to integrate UTC-PDs. In order to assess the effect of the impedance mismatch, a WR-10 (75 to 110 GHz) model was built and simulated on ANSYS HFSS. The insertion loss (IL) within the band is no larger than 1.5 dB and both the rectangular and GCPW ports present return losses above 10 dB. The input impedance of the transition was obtained from the extracted S-matrix and the resulting reflection coefficient and the losses related to the impedance mismatch were calculated following equation 2 and 3 for two different source impedances: a) 50 Ω GCPW and b) UTC-PD (Figure 2) with U_0=-1 V and respective photocurrents I_{ph}=8 mA and I_{ph}=16 mA. The resulting losses are plotted in Figure 5. It must be noted that the intrinsic IL of the transition is not accounted for in this calculation. A typical figure of merit for planar to rectangular waveguide transitions is the 3 dB-BW, i.e., the bandwidth in which the IL is lower than 3 dB with respect to the minimum IL within the band. By adding the losses due to impedance mismatch to the IL presented by the transition, it can be stated that the bandwidth of the transition is drastically reduced when using sources with complex impedances. For a photocurrent of 8 mA this results into losses of up to 3 dB as visible in Figure 5 (red dashed curve). However, in this particular case further increased photocurrent of 16 mA leads to reduced maximal losses of 1.5 dB contributed by the major drop in imaginary part of impedance in Figure 2 b). While Figure 2 a) also reveals an increase in real part of impedance, the overall impedance approaches 50 Ω significantly reducing the impedance mismatch.

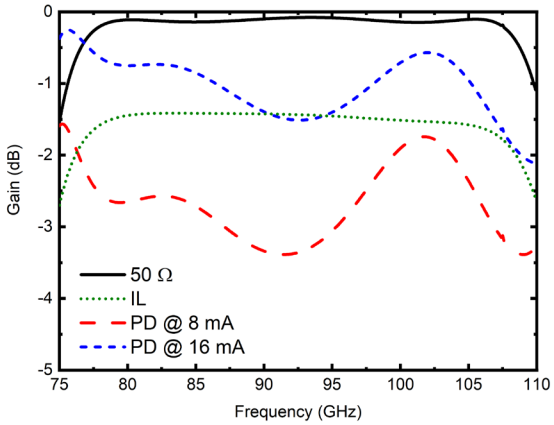

Fig. 5. Resulting transmission losses for an optimal 50 Ω port (black) and the simulated CPW integrated UTC-PD for two different photocurrents (dashed red and blue). Insertion losses of the transition are also included (dotted green).

III. Conclusions

In this work, we have highlighted the importance of properly modelling and matching the impedance of UTC-PDs. The paper shows the relevance of increasing the optical power by estimating a variation in the device's impedance. The presented method can be helpful when the measurement setup for network analysis can be too complicated when requiring optical coupling. By illustrating the behaviour of the carrier accumulation in the intrinsic region using the aforementioned equivalent circuit, the actual impedance can be approximated for the measured S-Parameter. Additionally, the applied bias voltage influences the built up or increase in capacitance as well. A higher bias or increased electric reduced carrier screening at high photocurrents leading to a slower built up in capacitance. Limitations of this approach can arise when certain interlayers are inserted to additionally improve the stability of the electric field. This can lead to inaccurate results for the calculated impedance. Furthermore, the importance of matching the device's impedance when integrating it with planar-to-rectangular waveguide transitions is illustrated by an example from a work found in literature. The presented simulation illustrates the relevance of knowing the performance depending impedance of such a device when designing a transition for maximized gain for the targeted frequency band.

Acknowledgment

M.G. would like to thank the Department of Optoelectronics at University of Duisburg-Essen for supporting this research. C.B would like to thank the FPU

Program from the Spanish Ministry of Science and, Innovation and Universities (FPU18/00013).

REFERENCES

[1] T. Ishibashi and H. Ito, "Uni-traveling-carrier photodiodes", Journal of Applied Physics 127, 031101, pp 1-10. January 2020. doi:10.1063/1.5128444

[2] Michele Natrella, Chin-Pang Liu, Chris Graham, Frederic van Dijk, Huiyun Liu, Cyril C. Renaud, and Alwyn J. Seeds, "Accurate equivalent circuit model for millimetre-wave UTC photodiodes," Opt. Express vol. 24, pp. 4698-4713, 2016.

[3] Y. -. Wu, J. -. Shi and P. -. Chiu, "Analytical modeling of a high-performance near-ballistic uni-traveling-carrier photodiode at a 1.55-μm wavelength," in IEEE Photonics Technology Letters, vol. 18, no. 8, pp. 938-940, April 2006, doi: 10.1109/LPT.2006.873567.

[4] C. C. Renaud, M. Natrella, C. Graham, J. Seddon, F. Van Dijk and A. J. Seeds, "Antenna Integrated THz Uni-Traveling Carrier Photodiodes," in IEEE Journal of Selected Topics in Quantum Electronics, vol. 24, no. 2, pp. 1-11, March-April 2018, Art no. 8500111, doi: 10.1109/JSTQE.2017.2725444.

[5] J. Li, B. Xiong, C. Sun, D. Miao, and Y. Luo, "Analysis of frequency response of high power MUTC photodiodes based on photocurrent-dependent equivalent circuit model," Opt. Express 23, 21615-21623, 2015.

[6] Michele Natrella, Chin-Pang Liu, Chris Graham, Frederic van Dijk, Huiyun Liu, Cyril C. Renaud, and Alwyn J. Seeds, "Accurate equivalent circuit model for millimetre-wave UTC photodiodes," Opt. Express 24, 4698-4713, 2016

[7] H. Song, K. Ajito, Y. Muramoto, A. Wakatsuki, T. Nagatsuma and N. Kukutsu, "Uni-Travelling-Carrier Photodiode Module Generating 300 GHz Power Greater Than 1 mW," in IEEE Microwave and Wireless Components Letters, vol. 22, no. 7, pp. 363-365, July 2012, doi: 10.1109/LMWC.2012.2201460.

[8] H. Ito, T. Ito, Y. Muramoto, T. Furuta and T. Ishibashi, "Rectangular waveguide output unitraveling-carrier photodiode module for high-power photonic millimeter-wave generation in the F-band," in Journal of Lightwave Technology, vol. 21, no. 12, pp. 3456-3462, Dec. 2003, doi: 10.1109/JLT.2003.821747.

[9] X. Shen et al., "High-Power V-Band-to-G-Band Photonically Driven Electromagnetic Emitters," in IEEE Transactions on Microwave Theory and Techniques, vol. 69, no. 2, pp. 1474-1487, Feb. 2021, doi: 10.1109/TMTT.2020.3044565.

[10] K. Sun, J. Moody, Q. Li, S. M. Bowers and A. Beling, "High Power Integrated Photonic W-Band Emitter," in IEEE Transactions on Microwave Theory and Techniques, vol. 66, no. 3, pp. 1668-1677, March 2018, doi: 10.1109/TMTT.2017.2755008.

[11] Grasser, Tibor, et al. "A review of hydrodynamic and energy-transport models for semiconductor device simulation." *Proceedings of the IEEE* 91.2 (2003): 251-274.

[12] Yang, Kyounghoon, Jack R. East, and George I. Haddad. "Numerical modeling of abrupt heterojunctions using a thermionic-field emission boundary condition." *Solid-State Electronics* 36.3 (1993): 321-330.

[13] Besher Khani, Sumer Makhlouf, Andreas G. Steffan, Jörg Honecker, and Andreas Stöhr, "Planar 0.05–1.1 THz Laminate-Based Transition Designs for Integrating High-Frequency Photodiodes With Rectangular Waveguides," J. Lightwave Technol. 37, 1037-1044 (2019)